9846 *Inorg. Chem.* **2009**, *48*, 9846–9852
DOI: 10.1021/ic901419w

Inorganic Chemistry
Article

Chloro and Azido Diruthenium Complexes Bearing Electron-Rich *N,N′,N′*-Triphenylguanidinate Ligands

József S. Pap, Jamie L. Snyder, Paula M. B. Piccoli, and John F. Berry*

Department of Chemistry, University of Wisconsin, 1101 University Avenue, Madison, Wisconsin 53706

Received July 20, 2009

The reaction of $Ru_2(OAc)_4Cl$ with *N,N′,N′*-triphenylguanidine (HTPG) produces one of two different compounds depending on the reaction conditions. In acetone in the presence of triethyl amine, the reaction produces tri-substituted $Ru_2(TPG)_3(OAc)Cl$, and in refluxing xylene, the tetra-substituted $Ru_2(TPG)_4Cl$ is produced. Both of these new complexes can be cleanly converted into their corresponding azido analogues by reaction with sodium azide in methanol. The X-ray crystal structures of $Ru_2(TPG)_3(OAc)Cl$, $Ru_2(TPG)_3(OAc)N_3$, and $Ru_2(TPG)_4Cl$ are presented, along with magnetic, electrochemical, and spectral measurements for each compound. Studies in solution show that, in contrast to $Ru_2(TPG)_3(OAc)Cl$, $Ru_2(TPG)_4Cl$ is sterically hindered at the axial positions, and readily dissociates a chloride ion at high ionic strength. Equilibrium constants for chloride association and dissociation have been estimated. Mass spectrometric data suggest that the two azido complexes are precursors to new diruthenium nitrido species.

Introduction

Metal−metal bonded diruthenium complexes are currently of interest because of their rich redox,[1−3] optical,[1a,b,2a−2c,4−6] and magnetic[7−12] properties. In particular, the ability of the Ru_2^{n+} core to adopt a large number of stable oxidation states ranging from Ru_2^{4+} to Ru_2^{7+} species has prompted investigations into the use of these compounds as catalysts for redox reactions.[13−15] To gain new insights into oxidative transformations enabled by diruthenium complexes, we have recently initiated a study of the high-valent chemistry of Ru−Ru bonded compounds and have isolated a remarkable nitrido species **II** with delocalized Ru−Ru−N σ and π bonds in the low temperature photolysis of the tetra-formamidinato diruthenium azido species $Ru_2(DPhF)_4N_3$ **I** (DPhF is the anionic ligand **III**, Scheme 1).[16] Our efforts to investigate the

*To whom correspondence should be addressed. E-mail: berry@chem.wisc.edu.

(1) (a) Ren, T. *Coord. Chem. Rev.* **1998**, *175*, 43. (b) Lin, C.; Ren, T.; Valente, E. J.; Zubkowski, J. D.; Smith, E. T. *Chem. Lett.* **1997**, 753. (c) Xi, B.; Ren, T. *C. R. Chim.* **2009**, *12*, 321. (d) Mahapatro, A. K.; Ying, J. W.; Ren, T.; Janes, D. B. *Nano Lett.* **2008**, *8*, 2131. (e) Lin, C.; Ren, T.; Valente, E. J.; Zubkowski, J. D. *J. Organomet. Chem.* **1999**, *579*, 114.

(2) (a) Kadish, K. M.; Wang, L. L.; Thuriere, A.; Van Caemelbecke, E.; Bear, J. L. *Inorg. Chem.* **2003**, *42*, 834. (b) Kadish, K. M.; Phan, T. D.; Giribabu, L.; Shao, J. G.; Wang, L. L.; Thuriere, A.; Van Caemelbecke, E.; Bear, J. L. *Inorg. Chem.* **2004**, *43*, 1012. (c) Kadish, K. M.; Wang, L. L.; Thuriere, A.; Giribabu, L.; Garcia, R.; Van Caemelbecke, E.; Bear, J. L. *Inorg. Chem.* **2003**, *42*, 8309. (d) Nakanishi, T.; Thuriere, A.; Bear, J. L.; Kadish, K. M. *Electrochem. Solid State Lett.* **2004**, *7*, E6.

(3) Collman, J. P.; Prodolliet, J. W.; Leidner, C. R. *J. Am. Chem. Soc.* **1986**, *108*, 2916.

(4) Miskowski, V. M.; Gray, H. B. *Inorg. Chem.* **1988**, *27*, 2501.

(5) Wesemann, J. L.; Chisholm, M. H. *Inorg. Chem.* **1997**, *36*, 3258.

(6) (a) Estiu, G.; Cukiernik, F. D.; Maldivi, P.; Poizat, O. *Inorg. Chem.* **1999**, *38*, 3030. (b) Castro, M. A.; Roitberg, A. E.; Cukiernik, F. D. *Inorg. Chem.* **2008**, *47*, 4682.

(7) Aquino, M. A. S. *Coord. Chem. Rev.* **1998**, *170*, 141.

(8) Mikuriya, M.; Yoshioka, D.; Handa, M. *Coord. Chem. Rev.* **2006**, *250*, 2194.

(9) (a) Liao, Y.; Shum, W. W.; Miller, J. S. *J. Am. Chem. Soc.* **2002**, *124*, 9336. (b) Shum, W. W.; Liao, Y.; Miller, J. S. *J. Phys. Chem. A* **2004**, *108*, 7460. (c) Vos, T. E.; Liao, Y.; Shum, W. W.; Her, J. H.; Stephens, P. W.; Reiff, W. M.; Miller, J. S. *J. Am. Chem. Soc.* **2004**, *126*, 11630. (d) Vos, T. E.; Miller, J. S. *Angew. Chem., Int. Ed.* **2005**, *44*, 2416. (e) Shum, W. W.; Her, J. H.; Stephens, P. W.; Lee, Y. J.; Miller, J. S. *Adv. Mater.* **2007**, *19*, 2910. (f) Kennon, B. S.; Her, J. H.; Stephens, P. W.; Shum, W. W.; Miller, J. S. *Inorg. Chem.* **2007**, *46*, 9033. (g) Shum, W. W.; Schaller, J. N.; Miller, J. S. *J. Phys. Chem. C* **2008**, *112*, 7936. (h) Her, J. H.; Kennon, B. S.; Shum, W. W.; Stephens, P. W.; Miller, J. S. *Inorg. Chim. Acta* **2008**, *361*, 3462.

(10) (a) Miyasaka, H.; Izawa, T.; Takahashi, N.; Yamashita, M.; Dunbar, K. R. *J. Am. Chem. Soc.* **2006**, *128*, 11358. (b) Motokawa, N.; Miyasaka, H.; Yamashita, M.; Dunbar, K. R. *Angew. Chem., Int. Ed.* **2008**, *47*, 7760. (c) Motokawa, N.; Oyama, T.; Matsunaga, S.; Miyasaka, H.; Sugimoto, K.; Yamashita, M.; Lopez, N.; Dunbar, K. R. *Dalton Trans.* **2008**, 4099.

(11) (a) Barral, M. C.; Gallo, T.; Herrero, S.; Jiménez-Aparicio, R.; Torres, M. R.; Urbanos, F. A. *Inorg. Chem.* **2006**, *45*, 3639. (b) Barral, M. C.; Jiménez-Aparicio, R.; Perez-Quintanilla, D.; Priego, J. L.; Royer, E. C.; Torres, M. R.; Urbanos, F. A. *Inorg. Chem.* **2000**, *39*, 65. (c) Jiménez-Aparicio, R.; Urbanos, F. A.; Arrieta, J. M. *Inorg. Chem.* **2001**, *40*, 613. (d) Barral, M. C.; Herrero, S.; Jiménez-Aparicio, R.; Torres, M. R.; Urbanos, F. A. *Angew. Chem., Int. Ed.* **2005**, *44*, 305.

(12) (a) Angaridis, P.; Berry, J. F.; Cotton, F. A.; Murillo, C. A.; Wang, X. *J. Am. Chem. Soc.* **2003**, *125*, 10327. (b) Chen, L.; Ramsey, C. M.; Dalal, N. S.; Ren, T.; Cotton, F. A.; Wernsdorfer, W.; Chiorescu, I. *Appl. Phys. Lett.* **2006**, *89*, 252502.

(13) Maas, G. *Top. Curr. Chem.* **1987**, *137*, 75.

(14) Komiya, N.; Nakae, T.; Sato, H.; Naota, T. *Chem. Commun.* **2006**, 4829.

(15) (a) Barker, J. E.; Ren, T. *Inorg. Chem.* **2008**, *47*, 2264. (b) Lee, H. B.; Ren, T. *Inorg. Chim. Acta* **2009**, *362*, 1467.

(16) Pap, J. S.; DeBeer, G. S.; Berry, J. F. *Angew. Chem., Int. Ed.* **2008**, *47*, 10102.

Published on Web 09/25/2009

Scheme 1

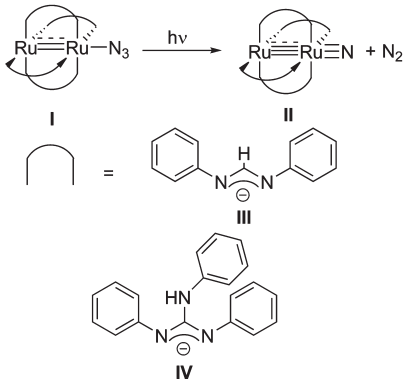

chemistry of this novel nitrido species have thus far been hindered by the inherent instability of **II**, as well as the limited solubility of **I**. Reported herein are our first efforts at overcoming these obstacles by using a new bridging ligand, *N*,*N*′, *N*″-triphenylguanidinate (TPG, **IV**).

The TPG ligand was chosen because it has been shown to stabilize metal−metal multiply bonded compounds in exceptionally high oxidation states[17,18] and because many of the $M_2(TPG)_4$ compounds are known to have good solubility in a range of organic solvents.[17,19,18,20] A ruthenium complex of the TPG ligand has already been described, $Ru(TPG)_3$, which is an octahedral tris-chelate of Ru(III).[21] It was, therefore, doubtful whether a metal−metal bonded diruthenium species could be formed with this ligand. Nevertheless, we show in this report that such a species, $Ru_2(TPG)_4Cl$ (**2**), can be formed in good yield. Its X-ray crystal structure, electrochemical and optical properties are described herein, as well as those of a partially substituted species, $Ru_2(TPG)_3(OAc)Cl$ (**1**), along with the corresponding azido derivatives of both (**4** and **3**, respectively).

Experimental Section

Materials. Ruthenium chloride ($RuCl_3 \cdot xH_2O$), lithium chloride, *N*,*N*′,*N*″-triphenylguanidine (HTPG), triethylamine (Et_3N), and the solvents were purchased from commercial sources. $Ru_2(OAc)_4Cl$ was prepared according to a published procedure.[22] Solvents were further purified either with a VAC Atmospheres Solvent Purification System or by standard methods; Et_3N was distilled under a nitrogen atmosphere before use.

Instrumentation. IR spectra were measured on a Bruker Tenser 27 FTIR Spectrometer using the KBr pellet technique. The Matrix-Assisted Laser Desorption/Ionization (MALDI) mass spectra were obtained using a Bruker REFLEX II (Billerica, MA) equipped with a 337 nm laser, a reflectron, and delayed extraction. In the positive ion mode, the acceleration voltage was 25 kV, and a time-of-flight (TOF) analyzer was used. Cyclic voltammograms (CV) were taken on a BAS Epsilon-EC instrument using CH_2Cl_2 solutions with 0.1 M NBu_4PF_6 and 1 mM of the compound of interest unless otherwise described (vide infra). The electrodes were as follows: glassy carbon (working), Pt wire (auxiliary), and either Ag/AgCl or $Ag/AgNO_3$ (reference). The potentials were referenced versus the ferrocene/ferrocenium redox couple, by externally added ferrocene. Electronic spectra were measured with a Varian Cary 50 Scan UV−visible spectrophotometer. Room temperature magnetic susceptibility measurements were performed on an Alfa Aesar magnetic susceptibility balance Mark 1, and corrected for inherent diamagnetism using Pascal's constants.[23] Electron Paramagnetic Resonance (EPR) spectra were measured on a Bruker Instruments E500A CW EPR spectrometer at a microwave frequency of 9.45 GHz.

Syntheses. $Ru_2(TPG)_3(OAc)Cl$ (1). A combination of 0.10 g of $Ru_2(OAc)_4Cl$ (0.21 mmol), 0.090 g of LiCl (2.1 mmol), and 0.480 g of HTPG (1.68 mmol) was dried in a Schlenk-flask at 100 °C, under vacuum for at least 1 h. Degassed acetone (25 mL) containing 120 μL of Et_3N was added to the solids at room temperature. The reaction mixture was heated to 75 °C and refluxed for 24 h during which time a dark green microcrystalline solid formed. The solid was filtered off from the olive green filtrate and washed with acetone (3 × 20 mL), water (3 × 10 mL) and with acetone again (3 × 10 mL) and air-dried. Yield: 0.22 g (90%) olive green, crystalline solid. Crystals suitable for X-ray crystallography were obtained from a CH_2Cl_2 solution of **1** that was layered with hexanes and slowly evaporated after the hexanes phase was completely mixed with the CH_2Cl_2. Anal. Calcd for $C_{59}H_{51}N_9O_2Ru_2Cl \cdot CH_2Cl_2$: C, 58.1; H, 4.3; N, 10.2. Found: C, 58.8; H, 4.4; N, 10.3. FT-IR bands (KBr pellet, cm^{-1}) 3389(m), 3057(w), 1593(m), 1521(s), 1486(s), 1419(s), 1266(m), 1076(w), 925(w), 749(m), 692(m). UV−vis (CH_2Cl_2) [λ_{max}, nm (ε, L mol^{-1} cm^{-1})] 440 (5,400), 720 (2,100). MALDI-TOF (pos. mode) in solid anthracene matrix: *m*/*z* for $[\mathbf{1}-Cl]^+$ 1121, for $[\mathbf{1}]^+$ 1156.

$Ru_2(TPG)_4Cl$ (2). A mixture of 0.10 g of $Ru_2(OAc)_4Cl$ (0.21 mmol), 0.090 g of LiCl (2.1 mmol), and 0.480 g of HTPG (1.68 mmol) was dried in a Schlenk-flask at 100 °C for 1 h, and then xylenes (30 mL) were added to the solids under a nitrogen atmosphere. A Soxhlet extractor was applied onto the flask together with a reflux condenser, and the Soxhlet thimble was charged with ∼1 g of dry potassium carbonate. The reaction mixture was then heated to 210−230 °C and refluxed for 24 h during which time a golden-yellow solid precipitated from the green solution. The solid was filtered off and washed with a tetrahydrofuran/water mixture (10 mL), water (2 × 10 mL), with cold methanol (5 mL), and finally with diethyl ether (5 mL) and was air-dried. Yield: 0.21 g (72%) golden-brown crystalline solid. Crystals suitable for X-ray crystallography were obtained from a dichloromethane solution of **2** layered with hexanes. Anal. Calcd for $C_{76}H_{64}N_{12}Ru_2Cl$: C, 66.0; H, 4.7; N, 12.2. Found: C, 66.0; H, 4.4; N, 12.1. FT-IR bands (KBr pellet, cm^{-1}) 3394(m), 3054(w), 1603(m), 1593(m), 1530(s), 1485(s), 1410(s), 1265(s), 1078(w), 927(w) 788(m), 758(m), 697(m). UV−vis (CH_2Cl_2) [λ_{max}, nm (ε, L mol^{-1} cm^{-1})] 768 (3,300), 432 (6,700). MALDI-TOF (pos. mode) in solid anthracene matrix: *m*/*z* for $[\mathbf{2}-Cl]^+$ 1348, for $[\mathbf{2}]^+$ 1383.

$Ru_2(TPG)_3(OAc)N_3$ (3). To a solution of 0.080 g (0.069 mmol) of **1** dissolved in CH_2Cl_2 (40 mL) and 3 mL of methanol was added 0.20 g (3.0 mmol) of NaN_3. The color of the solution changed from green to purple-brown. The mixture was stirred at room temperature overnight and then filtered. The solid was extracted with CH_2Cl_2 (2 × 40 mL), and the solution was evaporated to dryness in a rotary evaporator. The dark residue

(17) (a) Bailey, P. J.; Bone, S. F.; Mitchell, L. A.; Parsons, S.; Taylor, K. J.; Yellowlees, L. J. *Inorg. Chem.* **1997**, *36*, 867. (b) Bailey, P. J.; Bone, S. F.; Mitchell, L. A.; Parsons, S.; Taylor, K. J.; Yellowlees, L. J. *Inorg. Chem.* **1997**, *36*, 5420.

(18) Berry, J. F.; Bothe, E.; Cotton, F. A.; Ibragimov, S. A.; Murillo, C. A.; Villagrán, D.; Wang, X. *Inorg. Chem.* **2006**, *45*, 4396.

(19) Bailey, P. J.; Pace, S. *Coord. Chem. Rev.* **2001**, *214*, 91.

(20) (a) Cotton, F. A.; Daniels, L. M.; Huang, P.; Murillo, C. A. *Inorg. Chem.* **2002**, *41*, 317. (b) Cotton, F. A.; Dalal, N. S.; Hillard, E. A.; Huang, P. L.; Murillo, C. A.; Ramsey, C. M. *Inorg. Chem.* **2003**, *42*, 1388.

(21) Bailey, P. J.; Grant, K. J.; Mitchell, L. A.; Pace, S.; Parkin, A.; Parsons, S. *J. Chem. Soc., Dalton Trans.* **2000**, 1887.

(22) Stephenson, T. A.; Wilkinson, G. *J. Inorg. Nucl. Chem* **1966**, *28*, 2285.

(23) (a) Bain, G. A.; Berry, J. F. *J. Chem. Educ.* **2008**, *85*, 532. (b) O'Connor, C. J. In *Progress in Inorganic Chemistry*; Lippard, S. J., Ed.; John Wiley & Sons, Inc.: New York, 1982; Vol. *29*, p 203.

Table 1. Crystal Structure Details for $1\cdot CH_2Cl_2$, $2\cdot 4CH_2Cl_2$, and $3\cdot 0.5H_2O$

	$1\cdot CH_2Cl_2$	$2\cdot 4CH_2Cl_2$	$3\cdot 0.5H_2O$
chemical formula	$C_{59}H_{51}N_9O_2Ru_2Cl\cdot CH_2Cl_2$	$C_{76}H_{64}N_{12}Ru_2Cl\cdot 4CH_2Cl_2$	$C_{59}H_{51}N_{12}O_2Ru_2\cdot 0.5H_2O$
formula weight	1240.60	1722.69	1171.27
space group	triclinic, $P\bar{1}$	tetragonal, $P4/n$	monoclinic, $C2/c$
a, Å	10.909(2)	18.409 (5)	20.526 (3)
b, Å	16.533(3)	18.409 (5)	14.431 (3)
c, Å	17.406(3)	11.110 (3)	35.793 (6)
α, deg	117.755(3)	90	90
β, deg	102.374(3)	90	105.605 (4)
γ, deg	92.495(3)	90	90
V, Å^3	2675.9(9)	3764.7 (17)	10211 (3)
Z	2	2	8
D_{calc}, Mg m^{-3}	1.540	1.520	1.524
temperature, K	100 (2)	100 (2)	100 (2)
unique reflections	10791	4122	12627
data > 2σ/parameters/ restraints	7971/ 709/ 13	3617/ 263/ 4	11306/ 684/ 1
R1[a] [$F^2 > 2\sigma(F^2)$], wR2[b] (F^2)	0.060, 0.151	0.027, 0.089	0.035, 0.091
goodness of fit	1.06	1.20	1.16

[a] $R1 = \sum||F_o| - |F_c||/\sum|F_o|$. [b] $wR2 = [\sum w(F_o^2 - F_c^2)^2/\sum w(F_o^2)^2]^{1/2}$, $w = 1/\sigma^2(F_o^2) + (aP)^2 + bP$, where $P = [\max(0 \text{ or } F_o^2) + 2(F_c^2)]/3$.

was washed with a minimal amount of methanol and dried under vacuum. Yield: 0.070 g (85%) of purple solid. Crystals of **3** suitable for X-ray crystallography were obtained from a dichloromethane/hexanes mixture that was slowly evaporated under a nitrogen stream. Anal. Calcd for $C_{59}H_{51}N_{12}O_2Ru_2\cdot H_2O$: C, 60.0; H, 4.5; N, 14.2. Found: C, 59.3; H, 4.5; N, 14.3. FT-IR bands (KBr pellet, cm^{-1}) 3384(w), 3057(w), 2036(s), 1593(m), 1524(s), 1486(s), 1422(s), 1266(s), 928(w), 783(m), 692(m). UV−vis (CH_2Cl_2) [λ_{max}, nm (ε, L mol^{-1} cm^{-1})] 509 (6,400), 636 (2,900), 740 (sh). MALDI-TOF (pos. mode) in solid anthracene matrix: m/z for $[\mathbf{3}-N_3]^+$ 1121, $[\mathbf{3}-N_2]^+$ 1135.

$Ru_2(TPG)_4N_3$ (4). To a solution of 0.060 g (0.043 mmol) of **1** dissolved in CH_2Cl_2 (30 mL) and 2 mL of methanol was added 0.20 g (3.0 mmol) of NaN_3. The color of the solution changed from green to purple-brown. The mixture was stirred at room temperature overnight and then filtered. The purple solid was extracted with copious amounts of CH_2Cl_2 until the filtrate was colorless, and the combined filtrates were evaporated to dryness in a rotary evaporator. The resulting dark residues were washed with a minimal amount of methanol and dried under vacuum. Yield: 0.04 g (65%) of purple solid. Anal. Calcd for $C_{76}H_{64}N_{15}Ru_2$: C, 65.7; H, 4.6; N, 15.1 Found: C, 66.0; H, 4.5; N, 15.1. FT-IR bands (KBr pellet, cm^{-1}): 3398(w), 3057(w), 2067(s), 1593(m), 1529(s), 1485(s), 1414(s), 1264(s), 926(w), 784(w), 757(m), 697(m). MALDI-TOF (pos. mode) in solid anthracene matrix: m/z for $[\mathbf{4}-N_3]^+$ 1348, $[\mathbf{4}-N_2]^+$ 1362.

X-ray Crystallography. The crystal evaluations and data collections were performed on a Bruker SMART-1000 CCD diffractometer with graphite-monochromated Mo Kα (λ = 0.71073 Å) radiation. A green plate with approximate dimensions 0.44 × 0.12 × 0.10 mm^3 of $1\cdot CH_2Cl_2$, a brown block with dimensions 0.58 × 0.23 × 0.20 mm^3 of $2\cdot 4CH_2Cl_2$, and a brown block with dimensions 0.51 × 0.28 × 0.20 mm^3 of $3\cdot 0.5H_2O$ were selected under oil under ambient conditions and attached to the tip of a nylon loop. The crystals were mounted in a stream of cold nitrogen at 100(2) K and centered in the X-ray beam using a video camera.

A full sphere of data was collected to a resolution of 0.80 Å for $1\cdot CH_2Cl_2$, 0.78 Å for $2\cdot 4CH_2Cl_2$, and 0.75 Å for $3\cdot 0.5H_2O$. A total of 28302, 46706, and 64708 data were harvested, respectively, by collecting three sets of frames with 0.3° scans in ω and one set with 0.45° scans in φ. These highly redundant data sets were corrected for Lorentz and polarization effects. The absorption correction in each case was based on fitting a function to the empirical transmission surface as sampled by multiple equivalent measurements.[24] Relevant crystal data are given in Table 1.

All three structures were solved by direct methods followed by iterative cycles of least-squares refinement and difference Fourier synthesis. All non-hydrogen atoms were refined with anisotropic displacement coefficients. All hydrogen atoms were included in the structure factor calculation at idealized positions and were allowed to ride on the neighboring atoms with relative isotropic displacement coefficients. The structures of $1\cdot CH_2Cl_2$, $2\cdot 4CH_2Cl_2$, and $3\cdot 0.5H_2O$ were solved in the space groups $P\bar{1}$, $P4/n$, and $C2/c$, which were chosen because of proper systematic absences in the data and/or the appearance of chemically reasonable and computationally stable results. Each structure contains disordered solvent molecules, CH_2Cl_2 in the case of **1** and **2**, and H_2O in the case of **3**.

Results and Discussion

Synthesis. Considering the structural similarity between TPG and formamidinate ligands such as **III**, our initial attempts at the synthesis of diruthenium TPG complexes were based on a protocol developed by Ren et al. for the synthesis of their formamidinate analogues.[1b] In this procedure, $Ru_2(OAc)_4Cl$ is heated with HTPG, LiCl, and a base (triethylamine) in refluxing acetone solution (Scheme 2, left). Instead of the expected tetra-substituted $Ru_2(TPG)_4Cl$ compound, this preparative method led to the formation of the tri-substituted species $Ru_2(TPG)_3(OAc)Cl$, **1**, in excellent yield (90%). More demanding conditions were found to be necessary for the synthesis of the more sterically crowded $Ru_2(TPG)_4Cl$, **2**, namely, reaction of $Ru_2(OAc)_4Cl$ with HTPG and LiCl in refluxing xylene at over 200 °C in a Soxhlet apparatus having the thimble charged with K_2CO_3, which effectively removes acetic acid from the reaction mixture (Scheme 2, right). The chloro ligands in **1** and **2** were substituted by azido ligands forming **3** and **4** via metathesis using an excess of sodium azide.[25]

Structures. Compounds **1**−**3** adopt a metal−metal bonded paddlewheel-type structure, as shown in Figure 1. Selected bond distances and angles can be found in Tables 2 and 3. The Ru−Ru bond distances range from 2.2921(4)−2.3039(7) Å for **1**−**3** (see Table 2) and are close to the

(24) *Bruker-AXS SADABS V.2.05, SAINT V.6.22, SHELXTL V.6.10 & SMART 5.622 Software Reference Manuals*; Bruker-AXS: Madison, WI, 2000−2003.

(25) Chen, W. Z.; De Silva, V.; Lin, C.; Abellard, J.; Marcus, D. M.; Ren, T. *J. Cluster Sci* **2005**, *16*, 151.

Scheme 2

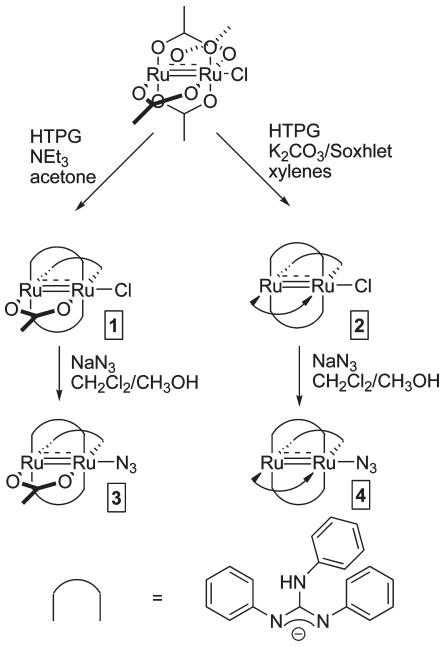

median Ru−Ru distance for paddlewheel complexes that do not possess carboxylate ligands (2.302 Å).[26,27] These distances are essentially equivalent within statistical error, indicating that neither the axial ligand nor the difference between TPG tri- or tetra-substitution has an effect on the Ru−Ru distance. Each complex is axially ligated on one end, with the opposite terminus free. Interestingly, in each structure, the −NHPh groups are arranged such that the phenyl rings are pointed away from the axially ligated side of the molecule. Also, the $Ru-L_{eq}$ distances are shorter for the terminally unligated Ru atom by approximately 0.02−0.05 Å than for the Ru atom that binds the terminal anion, a feature consistent with other Ru_2L_4X complexes as surveyed from the CSD.[27] This follows with the observation that as the coordination number at the metal atom increases, metal−ligand bond distances increase as well. The backbone of the guanidinate ligands is twisted by N−Ru−Ru−N torsion angles of approximately 13−19° (see Table 2), which are similar to those found in formamidinato compounds. Torsion angles for the OAc^- ligands are less than those for TPG, ostensibly because of the lack of bulky phenyl substituents on the ligand. The C−NH bond distances of ∼1.38 Å in the central planar N_3C unit of the TPG ligands indicate some C=N double bond character, which enhances the basicity of the TPG ligand relative to formamidinates. Complex **2** resides on a 4-fold crystallographic axis that is coaxial with the Ru−Ru bond that renders the TPG ligands equivalent by symmetry; complexes **1** and **3** are independent molecules in the asymmetric unit. The bite of the TPG ligand pulls the *trans* L−Ru−L angles in to be slightly less than 180° and the *cis* L−Ru−L angles around Ru fall in the range of 85−93°, which deviate from the ideal of 90° by more than do other $M_2(TPG)_4$ complexes.

(26) Angaridis, P. In *Multiple bonds between metal atoms*; Cotton, F. A., Murillo, C. A., Walton, R. A., Eds.; Springer Science and Business Media Inc.: New York, 2005.

(27) Allen, F. *Acta Crystallogr. B* **2002**, *58*, 380.

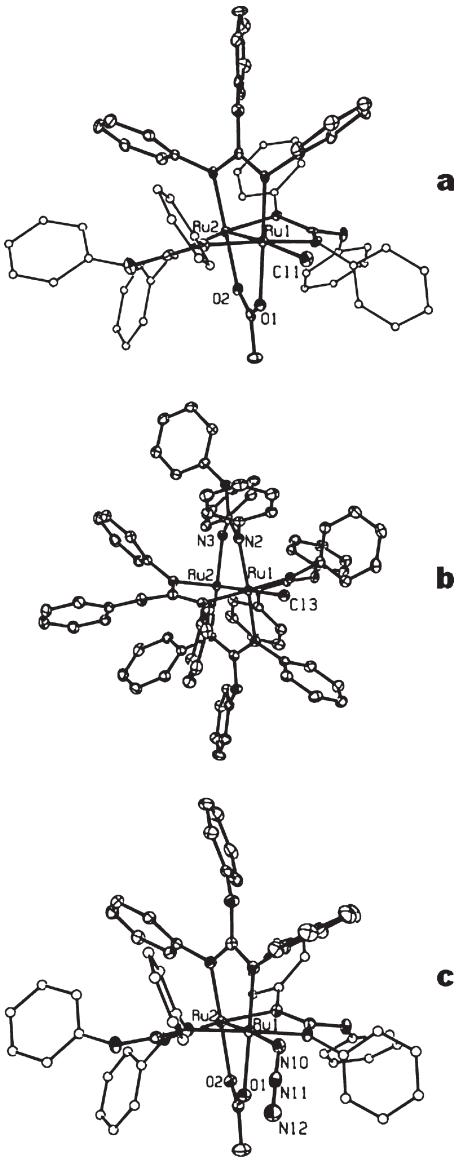

Figure 1. Molecular structures of **a** $1\cdot CH_2Cl_2$, **b** $2\cdot 4CH_2Cl_2$, and **c** $3\cdot 0.5H_2O$. Solvent molecules and hydrogen atoms have been removed for clarity. Some phenyl ring carbon atoms have also been plotted as spheres for viewing purposes. Ellipsoids have been plotted at the 50% probability.

Table 2. Selected Bond Distances (Å) for $1\cdot CH_2Cl_2$, $2\cdot 4CH_2Cl_2$, and $3\cdot 0.5H_2O$

atoms	$1\cdot CH_2Cl_2$	$2\cdot 4CH_2Cl_2$	$3\cdot 0.5H_2O$
Ru−Ru	2.2979(7)	2.3039(7)	2.2921(4)
Ru_1-L_{eq}	2.089[4], −N	2.098(2)	2.071[2], −N
	2.078(3), −O		2.091(2), −O
Ru_2-L_{eq}	2.035[4], −N	2.065(2)	2.049[2], −N
	2.052(3), −O		2.064(2), −O
Ru_1-L_{ax}	2.438(1)	2.434(1)	2.127(2)
N10−N11			1.190(3)
N11−N12			1.168(3)

Six other crystallographically characterized tetrakis TPG-subsituted metal−metal bonded compounds are known: $[Mo_2(TPG)_4]$ and $[Mo_2(TPG)_4][BF_4]$,[17] $[V_2(TPG)_4]$,[28]

(28) Cotton, F. A.; Hillard, E. A.; Murillo, C. A.; Wang, X. *Inorg. Chem.* **2003**, *42*, 6063.

Table 3. Selected Angles (deg) for $1 \cdot CH_2Cl_2$, $2 \cdot 4CH_2Cl_2$, and $3 \cdot 0.5H_2O$

atoms	$1 \cdot CH_2Cl_2$	$2 \cdot 4CH_2Cl_2$	$3 \cdot 0.5H_2O$
Ru2−Ru1−Cl_{ax}	175.44(4)	180.0	
Ru2−Ru1−N10			175.30(6)
Ru1−N10−N11			126.50(17)
N10−N11−N12			176.4(2)
N−Ru1−Ru2−N	15.93(12), N2/N3	18.79(5)	18.39(6), N2/N3
torsion	16.25(16), N5/N6		15.02(6), N5/N6
	18.04(13), N8/N9		14.09(6), N8/N9
	14.39(11), O1/O2		13.50(5), O1/O2

$[Rh_2(TPG)_4]$,[29] and $[Ni_2(TPG)_4]$ and $[Ni_2(TPG)_4][BF_4]$,[18] none of which contain axial ligands; compounds **1**−**3** are thus the first metal−metal bonded $M_2(TPG)_n$ (n = 3 or 4) complexes to be structurally characterized with an axially bound ligand. The torsion angles in these reported complexes fall into the same range as the ones reported here except for $[Mo_2(TPG)_4]$ and $[Mo_2(TPG)_4][BF_4]$, whose torsion angles fall close to zero, as expected from the δ bond present in those species. The Ru−Ru bond distances reported here for **1**− **3** of ∼2.30 Å fall nicely between those of $Mo_2(TPG)_4/Mo_2(TPG)_4^+$, 2.08/2.12 Å, and $Rh_2(TPG)_4$, 2.40 Å, in good agreement with a Ru−Ru bond order of 2.5.

Because of the inherent insolubility of **4**, we were unable to produce high quality crystals of the compound. A low resolution crystal structure was nevertheless obtained, which shows the expected atom connectivity of the molecule.[30] Although accurate bond distances cannot be derived from this structure, it should be noted that the terminal Ru−N3 group is linear with a Ru−N−N angle of 180°, in contrast to the bent structure of **3** (Ru−N−N = 127°).

Magnetic and EPR Measurements. Complexes **1**−**3** have room temperature magnetic moments (μ_{eff}) of 3.9, 3.6, and 3.8 μ_B ($\chi \cdot T$ = 1.90, 1.62, and 1.81 emu K mol^{-1}), respectively, which correspond to 3 unpaired electrons, consistent with other Ru_2^{5+} complexes containing carboxylate, formamidinate, and mixed ligands.[1b,26] Compound **4** consistently yields anomalously high room temperature magnetic moments, ≥ 5.6 μ_B, which vary widely depending on sample preparation and recrystallization. These high μ_{eff} values are likely due to the presence of a small amount of a highly paramagnetic impurity that, like **4**, is insoluble.

To gain a better understanding of the magnetic properties of **4** in the absence of impurities, we have examined a dilute solution of **4** in 4-*tert*-butyl pyridine by EPR spectroscopy. 4-*tert*-Butyl pyridine is the only solvent we have found so far in which **4** is sparingly soluble. The EPR spectrum of **4** in this solvent at 4 K is shown in Figure 2, and features an axial signal with $g_{\perp,eff}$ = 4.19 and $g_{||,eff}$ = 1.97. The axial symmetry of the EPR spectrum is in good agreement with the molecular symmetry of **4** and the effective g values of ∼4 and 2 indicate that the compound has an S = 3/2 ground spin state with $D \gg h\nu$. This observation is consistent with the expected $\sigma^2\pi^4\delta^2(\pi^*\delta^*)^3$ ground state and large zero-field splitting

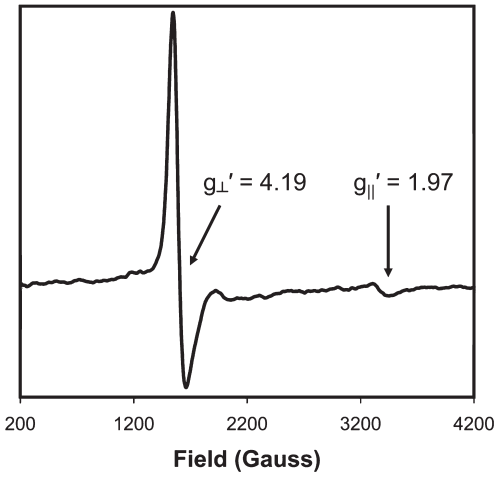

Figure 2. X-band EPR spectrum of **4** in frozen 4-*tert*-butyl pyridine solution at 4 K. Effective g values for the S = 3/2 system are indicated.

that have been determined for other Ru_2^{5+} complexes.[31] Compounds **1**−**3** have qualitatively similar CH_2Cl_2 solution EPR spectra (Supporting Information, Figures S1−S3), though the $g_\perp$ signal in the spectrum of **3** is flanked by satellite peaks that likely indicate dimerization or oligomerization.

Solution Behavior: Electronic Spectroscopy and Cyclic Voltammetry. Electronic spectra of $Ru_2(ligand)_4Cl$ species have been analyzed in detail by Miskowski and Gray.[4] Additionally, Ren has found that the lowest energy band in the visible region for a series of $Ru_2(formamidinate)_4Cl$ complexes is very sensitive to the electronic nature of the formamidinate ligand, and that this band undergoes a bathochromic shift as the formamidinate ligands become more electron rich.[1b] The lowest-energy band observed by Ren was for $Ru_2(DAniF)_4Cl$ (DAniF = di-*p*-anisylformamidinate) at 688 nm, and was assigned following the Miskowski and Gray formalism as a $Ru_2\ \delta \rightarrow Ru_2\ \pi^*$ transition.[1b] It is now well-known that there is significant overlap between ligand π orbitals and M_2 δ orbitals,[18,32] so the $\delta \rightarrow \pi^*$ assignment makes sense considering its variability with the electronic nature of the ligand.

Compound **1** is green in solution, with absorption features at 720 and 440 nm. Since the TPG ligand is known from previously reported electrochemical work[17,18] to be much more electron donating than the DAniF ligand used by Ren, it is reasonable to assign the low energy band at 720 nm to the $\delta \rightarrow \pi^*$ transition. This assignment signifies a greater electron-richness of TPG as compared to DAniF, in agreement with previous results on the corresponding dinickel compounds.[18] The $\delta \rightarrow \pi^*$ transition is shifted to even lower energy, ∼770 nm, for the tetra-substituted compound **2**. Addition of excess chloride ion to **2** causes a slight decrease in intensity of the $\delta \rightarrow \pi^*$ band indicative of the formation of $[Ru_2(TPG)_4Cl_2]^-$ (Supporting Information, Figure S4).[4]

Surprisingly, the electronic spectrum of **2** in CH_2Cl_2 solution is strongly affected by ionic strength (I). In the

(29) Lutterman, D. A.; Degtyareva, N. N.; Johnston, D. H.; Gallucci, J. C.; Eglin, J. L.; Turro, C. *Inorg. Chem.* **2005**, *44*, 5388.

(30) Crystal data for $4 \cdot CH_2Cl_2$: Tetragonal, space group $P4/n$, $a = b$ = 18.126(5) Å, c = 11.394(5) Å, V = 3743(2) $Å^3$, Ru−Ru = 2.297 Å.

(31) (a) Telser, J.; Drago, R. S. *Inorg. Chem.* **1984**, *23*, 3114. (b) Angaridis, P.; Cotton, F. A.; Murillo, C. A.; Villagrán, D.; Wang, X. P. *J. Am. Chem. Soc.* **2005**, *127*, 5008.

(32) (a) Berry, J. F.; Bill, E.; Bothe, E.; Cotton, F. A.; Dalal, N. S.; Ibragimov, S. A.; Kaur, N.; Liu, C. Y.; Murillo, C. A.; Nellutla, S.; North, J. M.; Villagrán, D. *J. Am. Chem. Soc.* **2007**, *129*, 1393. (b) Cotton, F. A.; Gruhn, N. E.; Gu, J. D.; Huang, P.; Lichtenberger, D. L.; Murillo, C. A.; Van Dorn, L. O.; Wilkinson, C. C. *Science* **2002**, *298*, 1971.

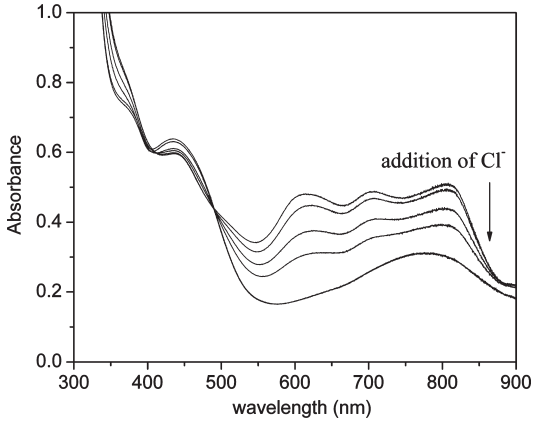

Figure 3. Absorption spectrum of **2** at a concentration of 0.1 mM in CH_2Cl_2 solution with 0.1 M NBu_4PF_6 and 0 mM, 0.1 mM, 0.5 mM, 1 mM, and 10 mM tetraethylammonium chloride added.

Scheme 3

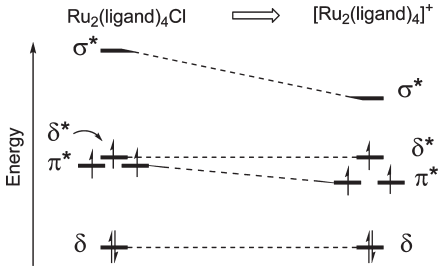

presence of 0.1 M NBu_4PF_6, instead of a single major absorption in the visible region, three bands of roughly equal intensity are observed at ~800 nm, 700 nm, and 600 nm (Figure 3). Upon addition of excess chloride ion to this solution, the spectrum simplifies to the original spectrum observed when $I = 0$ M. We therefore propose that the absorption features at 600, 700, and 800 nm are those associated with an unligated $[Ru_2(TPG)_4]^+$ species. To our knowledge, the electronic spectrum of a $[Ru_2(ligand)_4]^+$ cation devoid of axial ligation has not been analyzed. A complete assignment of the absorption spectrum is outside the scope of this work, but we suggest preliminary assignments of the 600 and 700 nm bands as either Ru_2 δ, π^*, or $\delta^* \rightarrow Ru_2$ σ^* transitions while the 800 nm band is the $\delta \rightarrow \pi^*$ transition. These assignments agree with the expected lowering of the Ru_2 σ^* and π^* orbitals in energy with loss of the axial chloro ligand (see Scheme 3, based on calculated molecular orbital diagrams from reference 26).

The discussion of the electronic spectra of **1** and **2** above helps us to interpret the electrochemical properties of these compounds. CVs of **1** and **2** are shown in Figure 4, where clear differences between the two compounds can be seen. The CV of **1** is similar to those of other $Ru_2(ligand)_4Cl$ complexes in that it displays a reversible oxidation at $E_{1/2} = 0.061$ V versus ferrocene to a $[Ru_2(TPG)_3(OAc)Cl]^+$ species and an irreversible reduction where electron transfer to form the $[Ru_2(TPG)_3(OAc)Cl]^-$ anion is followed quickly by chloride loss.[1b,33]

(33) Kadish, K. M.; Garcia, R.; Phan, T.; Wellhoff, J.; Van Caemelbecke, E.; Bear, J. L. *Inorg. Chem.* **2008**, *47*, 11423.

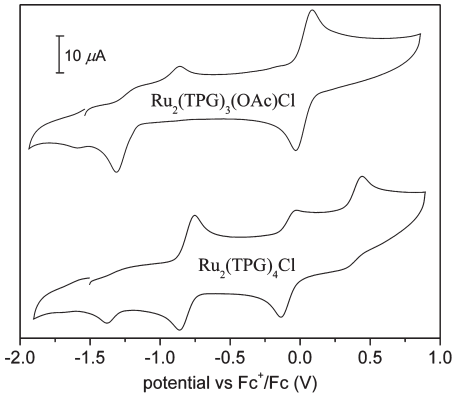

Figure 4. CVs of compounds **1** and **2** taken at a scan rate of 200 mV s^{-1} using a glassy carbon working electrode, Pt wire auxiliary electrode, and a $Ag/AgNO_3$ reference electrode. Potentials are referenced to the ferrocene/ferrocenium couple.

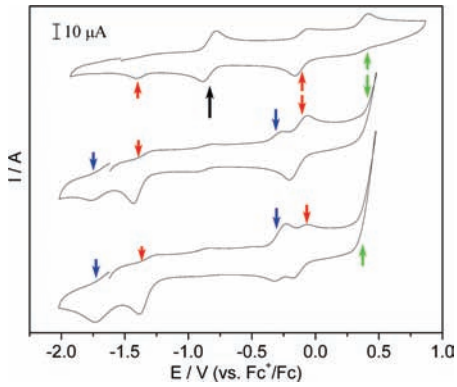

Figure 5. CVs of **2** in (top) 0.1 M NBu_4PF_6, (middle) with additional 10 mM NEt_4Cl/0.1 M NBu_4PF_6, and (bottom) 30 mM NEt_4Cl/0.1 M NBu_4PF_6 in CH_2Cl_2. Arrows are color-coded for the following redox processes: black, $[Ru_2(TPG)_4]^{n+}$; red, $[Ru_2(TPG)_4Cl]^{n+}$; blue, $[Ru_2(TPG)_4Cl_2]^{n+}$; green, Cl^-/Cl_2.

The oxidation of **1** to $\mathbf{1}^+$ is at a similar potential to the corresponding oxidation of $Ru_2(DPhF)_4Cl$ (DPhF = diphenylformamidinate), which occurs at 0.054 V versus ferrocene.[1b] The CV of **2** is complex, indicative of an ECE mechanism; to aid in its interpretation, CVs of **2** in the presence of 10 mM and 30 mM tetraethylammonium chloride were also measured, shown in Figure 5. With no chloride present, there is a quasireversible wave at $E_{1/2} = -828$ mV that vanishes upon addition of chloride ions and may therefore be assigned as the $[Ru_2(TPG)_4]^{+/0}$ wave. Additionally, a quasireversible $[Ru_2(TPG)_4Cl]^{+/0}$ wave at $E_{1/2} \sim -55$ mV and an irreversible $[Ru_2(TPG)_4Cl]^{0/-}$ wave a $E_{pc} \sim -1.35$ V are observed whose intensities increase as the chloride ion concentration increases. At high chloride ion concentrations, a new quasireversible wave at $E_{1/2} = -175$ mV along with an irreversible wave at $E_{pc} = -1.66$ V appear that may be assigned to the $[Ru_2(TPG)_4Cl_2]^{0/-}$ and $[Ru_2(TPG)_4Cl_2]^{-/2-}$ processes, respectively. These assignments, which are summarized in Scheme 4, are consistent with our expectation that (1) reductions of $[Ru_2(TPG)_4]^+$, $Ru_2(TPG)_4Cl$, and $[Ru_2(TPG)_4Cl_2]^-$ become successively more difficult by roughly 0.5 V as the charge on the molecule becomes more negative; (2) oxidation of $[Ru_2(TPG)_4Cl_2]^-$ is ~100 mV more accessible than for $Ru_2(TPG)_4Cl$; and (3) redox processes of **2** occur at more negative potentials than those of **1** because of the replacement of an acetate ligand in the

Scheme 4

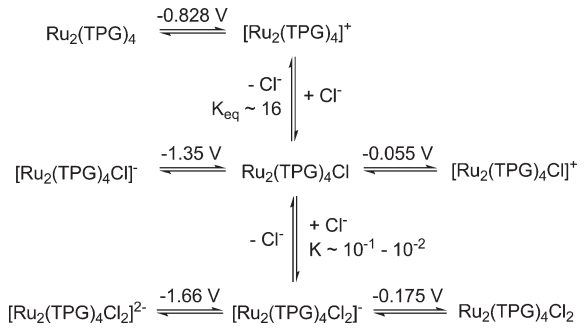

former for a guanidinate ligand in the latter. A similar observation to (3) has been made for a series of Ru_2 mixed acetate/amino-pyridinate complexes.[33]

Using the above assignments and the peak currents from the CVs of **2**, it is possible to estimate equilibrium constants for chloride binding to the $[Ru_2(TPG)_4]^+$ core at $I = 0.1$ M. Chloride dissociation from **2** follows the equilibrium in eq 1. The relative concentrations of all three species in this equilibrium, $[Ru_2(TPG)_4Cl]$, $[Ru_2(TPG)_4^+]$, and $[Cl^-]$, may be directly determined from the peak currents, which are proportional to concentration. Note that the Cl^- concentration can be determined from the irreversible wave for oxidation of Cl^- seen at 423 mV. Dissociation of Cl^- from **2** is therefore thermodynamically favorable with an equilibrium constant of ~16 at $I = 0.1$ M, which explains why new features attributable to $[Ru_2(TPG)_4]^+$ could be observed in the electronic spectrum of solutions of **2**.

$$Ru_2(TPG)_4Cl \rightleftharpoons [Ru_2(TPG)_4]^+ + Cl^- \qquad K_{eq} \sim 16. \tag{1}$$

By using a large excess of Cl^- ions in solution, we are able to determine the equilibrium constant for binding of Cl^- to **2** as shown in eq 2. Addition of a second chloride ion to the axial position of **2** is unfavorable at $I = 0.1$ M, presumably because of a combination of steric effects of the bulky TPG ligands, as well as electronic effects of the electron-rich TPG ligands that lower the Lewis acidity of the Ru_2 unit. More favorable chloride ion association is, however, observed at $I = 0$ M.

$$Ru_2(TPG)_4Cl + Cl^- \rightleftharpoons [Ru_2(TPG)_4Cl_2]^- \qquad K_{eq} = 10^{-1} - 10^{-2} \tag{2}$$

The electrochemical properties of **3** are somewhat similar to those of **1** in that the CV consists of a reversible oxidation wave ($Ru_2(TPG)_3(OAc)N_3 \rightleftharpoons [Ru_2(TPG)_3(OAc)N_3]^+$) at $E_{1/2} = 17$ mV and a multielectron reduction at −1.46 V (Supporting Information, Figure S5). Similarly to the case of **1**, the $\mathbf{3}^+/\mathbf{3}$ redox couple occurs at a similar potential to that of $Ru_2(DPhF)_4N_3$ at −0.03 V.[25] The electrochemical properties of **4** could not be determined because of its insolubility; we may expect, however, that its electrochemical profile will be similar to that of $Ru_2(TPG)_4Cl$, although with a lower oxidation potential to $\mathbf{4}^+$, and without any of the complications because of loss of the axial ligand.

Conclusions. Tri- and tetra-substituted triphenylguanidinate complexes utilizing the $[Ru_2]^{5+}$ core have been prepared, structurally characterized, and their solution behavior studied by UV−vis and cyclic voltammetry. These are the first $[M_2L_4]$ complexes containing the TPG ligand that are axially ligated. The chloride ion in $Ru_2(TPG)_4Cl$ easily dissociates at $I = 0.1$ M, suggesting that despite their similarities, the TPG ligand is more electron-rich and causes more steric crowding of the axial positions than does the DPhF ligand. Finally, preliminary MALDI-TOF experiments in positive-ion mode at high power on the azide complexes **3** and **4** show evidence of formation of the terminal nitrides $[Ru_2(TPG)_3(OAc)N]^+$ and $[Ru_2(TPG)_4N]^+$ at 1134.0 and 1362.0, respectively. This reactivity follows in line from experiments showing the generation of the terminal nitride $[Ru_2(DPhF)_4N]$ from corresponding azide $[Ru_2(DPhF)_4N_3]$[16] and warrants further study. The insolubility of **4** was unexpected and may hamper further investigation of its conversion to the corresponding nitrido compound.

Acknowledgment. We are grateful to the University of Wisconsin for financial support, and to the National Science Foundation funding for the EPR spectrometer (CHE-0741901). We thank Michael Nippe for obtaining the EPR spectra.

Supporting Information Available: X-ray crystallographic data for **1**−**3** in CIF format, and Figures S1−S5. This material is available free of charge via the Internet at http://pubs.acs.org.